Wiley
Advances in Civil Engineering
Volume 2024, Article ID 6220245, 13 pages
https://doi.org/10.1155/2024/6220245

WILEY

Research Article

Mapping Longitudinal and Transverse Displacements of a Dam Crest Based on the Synergy of High-Precision Remote Sensing

Fabiola D. Yépez-Rincón,[1] **Adrián L. Ferriño Fierro**,[1] **Andrea N. Escobedo Tamez**,[1] **Víctor H. Guerra Cobián**,[1] **Olmo E. Pinedo Sandoval**,[1] **Jorge H. Chávez Gómez**,[1] **Luis C. Alatorre Cejudo**,[2] **and Saied Pirasteh**[3,4]

[1]*Faculty of Civil Engineering, Universidad Autónoma de Nuevo León, San Nicolás de los Garza C.P.64455, Nuevo León, Mexico*
[2]*Organismo de Cuenca Río Bravo, Comisión Nacional del Agua, Av. Constitución 4103 Ote. Col. Fierro, Monterrey 64590, Nuevo León, Mexico*
[3]*Institute of Artificial Intelligence, Shaoxing University, 508 West Huancheng Road, Yuecheng District, Shaoxing Postal Code 312000, Zhejiang Province, China*
[4]*Department of Geotechnics and Geomatics, Saveetha School of Engineering, Saveetha Institute of Medical and Technical Sciences, Chennai Pin 602105, Tamil Nadu, India*

Correspondence should be addressed to Fabiola D. Yépez-Rincón; fabiola.yepezrn@uanl.edu.mx

Received 4 August 2023; Revised 29 April 2024; Accepted 3 May 2024; Published 28 May 2024

Academic Editor: Ahad Javanmardi

Reservoirs are highly relevant infrastructure assets, and now, more than ever, they play an essential role in society's welfare and national security. Their importance is related to regional socioeconomic development due to their capacity to store water for different uses, such as human consumption, agricultural irrigation, flood control, and hydroelectric energy production, among other important services. However, many reservoirs are reaching the end of their period of life, and others are showing undesired displacements and cracking. Four 3D surveys were conducted on a reservoir that serves the Metropolitan Area of Monterrey City in Mexico. These surveys were carried out over a period of 5 years using GNSS observation to assist in understanding the actual dam kinematics, i.e., the behavior of its longitudinal and transversal displacements and the possible correlation with the reservoir level. The high-precision leveling and close-range remote sensing data were assessed and then mapped. The high-precision geodetic and leveling techniques allowed us to locate and measure 84 established permanent control points with errors of about ± 0.003 m. The mapping of displacements was made possible by modeling the positive and negative translations. The highest uplifts (11 mm) occurred at the left riverbank, and the highest subsidences (−5 mm) occurred along the downstream piers from the middle of the dam crest to the right riverbank. A ground laser scanner (GLS) produced 3D digital models with geometrical and radiometric characteristics, detecting displacements among the dam crest elements. The synergy of GNSS and high-leveling techniques allows the possibility to measure displacements, while the use of geographical information system (GIS) and geomatic techniques allows a better visualization through 2D and 3D maps validated using traditional topographical methods.

1. Introduction

Hydraulic infrastructure is a national asset that allows the use and management of water resources and the control of floods (for the protection of the population) and functions as a strategic reserve for times of drought [1]. Dams provide societal benefits, namely drinking water, irrigation, and energy generation. Therefore, a possible failure in the system represents risks in the form of material losses to the environment, especially if they are close to urban communities. For example, in August 1975, Typhoon Nina struck Zhumadian in China's Henan province [2], causing extreme rainfall and surpassing the total annual precipitation in the area. The Banqiao dam failure was the most fatal failure dam event in history, with more than 170,000 deaths and millions of people homeless. Daowencheng, the closest town, was immediately inundated,

and almost 10,000 citizens were killed during the first few hours [3].

All possible causes of dam failures are considered during their design. Furthermore, the values or assumptions consider the theoretical stresses and deformations, which have to comply with fields such as balance, compatibility, boundary conditions, and material [4]. With these considerations, it is expected that the body of the structure remains continuous during deformation. If the dam does not present cracks or overlaps, it is important that the tensor meets the additional conditions of integrality and that those conditions are kinematically admissible [5].

As time goes on, climate change and pollution will significantly impact the safety of these hydraulic systems [6]. Deterioration factors, such as loads, thermal expansions, and contractions, decrease the structure's effectiveness [7]. Supervision and maintenance become indispensable [8] to understand if temporary or permanent displacements and deformations are due to gravitational loads, wind, earthquakes, or human activity [9].

Regular inspections could, in many cases, prevent failures. For example, in 2019, in Paraíba, Brazil, poor maintenance left 3,000 people homeless as a consequence of displacements exceeding the critical limits of the dam structure. Similar incidents around the world demonstrate how poor maintenance increases the risks from external factors such as heavy rain, among others, especially when a lack of inspection or illegal modifications occurs.

During the last few decades, dam safety has attracted increasing attention because of the high number of accidents and failures that have occurred [10]. The number of dam failures will increase, according to a study by the United Nations University [11]. By 2050, most people will live downstream of large dams built in the 20th century [12], many of which are approaching the limits of their useful lifetime.

Inspection and monitoring of dam infrastructure is a field that has been gaining attention in recent years, especially on dams that have exceeded their designed lifespan. This brings the challenge of obtaining high-precision information that is operationally feasible and at an affordable cost. According to FEMA [13], the process of dam monitoring consists of seven steps: surveillance, instrumentation, data acquisition, evaluation, analysis, management, and decision-making. Surveying and monitoring the static and dynamic behavior of large dams is and will be a topic of great interest and relevance due to the impact that these types of structures have on the landscape where they have been built [14]. Monitoring the structural response to detect abnormalities must be imperative. However, many governments are not prepared for these needs. The early detection of anomalies could focus on appropriate corrective actions [15].

According to the International Commission on Large Dams (ICOLD), the first criterion to define a large dam is that it has a height of 15 m or greater, measured from the lowest point of the foundation to the crest. The second criterion is a dam with a height between 5 and 15 m, impounding more than 3 mm^3 [10, 16]. In Mexico, over 4,400 dams were built by government agencies and private enterprises, with an approximate storage capacity of 150 mm^3. CONAGUA [17] reports that 667 dams (15%) correspond to large dams and store almost 80% of the reservoir water. These are important for Mexicans; nevertheless, most of the dams are close to the end of their operational life.

Several studies have used geodetic or geotechnical methods for dam monitoring, especially those using the Global Navigation Satellite System (GNSS) station time series. For example, Kalkan [18] monitored deformations of the Ataturk Dam from 2006 to 2010 using geodetic methods, where the monthly average radial velocity was found to be 2.2 mm. Other studies, such as Michalis et al. [19], used geodetic monitoring to measure horizontal and vertical displacements (crest settlements). They used a 29-year-long dataset of the Pournari I Dam in Greece and found that the displacements remained within normal limits for the analyzed time period. Grosel [20] used geotechnical monitoring to calibrate a genetic algorithm and predict deformations. Geotechnical values were the main data used to monitor and evaluate dam deformations. However, this model needed several runs to find the best fit.

Reservoir level fluctuations and their relationship to dam deformations have been studied by Yigit et al. [21]. This study revealed evidence that the reservoir level and the seasonal temperature variations are the main sources of the measured deformations in the Ermenek Dam in Turkey. Their results are based on the combination of conventional geodetic measurements and the finite element model (FEM). Galán-Martín et al. [22] successfully used a Differential Global Positioning System (DGPS) to monitor millimetric ($\pm$2–3 mm) movements of the La Aceña Dam in Spain. In 2022, Vazquez-Ontiveros et al. [23] used the GNSS reflectometry inversion technique to monitor 3.5 years of local deformations of the Sanalona Dam, a gravity-type dam located in Culiacan, Mexico. Their findings highly correlate (0.97) deformations of the crest with the reservoir level. Mapping displacements is a less explored field.

Even though there are some studies, such as the two-dimensional (2D) mapping using an interpolation method to simulate an uneven deformation rate, the interpolation method has been used in many fields of knowledge. Wang et al. [24] used a method based on the radial basis function for land cover mapping at the subpixel scale by hardening the soft class values. In ongoing research in autonomous vehicles, conventional LIDAR 3D data were transformed into 2D images by Ashraf et al. [25] by using an interpolation technique based on the density of the data. In physics, Yin et al. [26] used interpolation routines with parallel for-loops over query points to compute several numerical tests for the 3D incompressible Euler equations. Poreh and Pirasteh [27] reported vertical deformations and analyzed several CosmoSkyMed images utilizing the interferometric synthetic aperture radar (InSAR) technique to improve the understanding of 3D surface displacements. Later, Poreh et al. [28] used InSAR, Continuous Global Positioning Systems, and optical remote sensing data to analyze Mexico City's subsidence. Accordingly, in another study, Chen et al. [29] interpolated GPS data to obtain continuous spatial estimates of vertical deformations.

Three-dimensional (3D) models using ground laser scanners (GLS) have been applied to monitor dam deformation. Authors such as González-Aguilera et al. [30] concluded that the GLS alone is not sufficient to monitor dam displacements. Indeed, it is the necessary synergy of GLS and GPS. This way, the demanded level of precision can be attained and measured through time. Xu et al. [31] used GLS for earthen dams, and Li et al. [32] for arch dams. However, in almost all cases, highly accurate leveling techniques are used to validate the analysis. In order to understand the actual condition of a dam crest, it is necessary to monitor the behavior of vertical and horizontal displacements and their possible correlation with the reservoir level. Using the synergy of GPS observations, high-precision leveling and close-range remote sensing data were assessed and mapped. Herein are analyzed four 3D surveys made during a period of 5 years in a dam in the northeast of Mexico.

The contributions of this paper are as follows:

(i) A consistent, decisive, and stricter displacement monitoring method that enhances millimetric accuracy for longitudinal and transverse displacements was attained based on 2D and 3D models.

(ii) The data collected can be used to validate theoretical and numerical models of structural behavior, improving understanding of the actual conditions of the dam and the accuracy of predictions.

(iii) Studies employing these techniques offer essential information for the management, maintenance, and security of critical infrastructures such as dams, contributing to informed decision-making and the prevention of potential risks.

(iv) The ability to identify dam displacements even before they reach critical levels can be crucial for making preventive decisions and early warning.

2. Data and Methods

2.1. Case Study: Solidaridad "El Cuchillo" Dam. The Monterrey Metropolitan Area has a population of 5,195,000 people and is the second most populated metropolitan area in Mexico. The water supply for the population is carried out through three dams: Rodrigo Gómez "La Boca," José López Portillo "Cerro Prieto," and Solidaridad "El Cuchillo." Due to the reduction in precipitation levels in the northeastern region of Mexico, "El Cuchillo" plays an important role as a main reserve and represents a national security issue.

"El Cuchillo" dam site is located at 25°42′ N and 99°17′ W in China City, Nuevo León, in the northeast of México (Figure 1). It was built from 1990 to 1994 to supply drinking water and irrigation to the region. In 1994, the "El Cuchillo" Dam was put into operation, with a 1,123 mm^3 of storage capacity. It has an aqueduct of 110 km, is 2.13 m in diameter, and has 5 pumping stations with a capacity of 45,000 HP. Since its inception, it has been operated by Water and Sewer Services of Monterrey [33], and its primary function is water management for the distribution and supply of 5,000 L/s to the Metropolitan Area of Monterrey. The reservoir captures runoff from the San Juan River basin and has a dam of graduated materials, with slopes of a 2 : 1 ratio. The dam has a length of 10,800 m (Figure 1). This includes the portion of the gravity section where the excess spillway structures are located. That is 320.0 m long, 44.0 m maximum height from the ground, and 10.0 m wide crown at an elevation of 169.66 m above sea level (m.a.s.l.). Seven radial gates control the surplus spillway, which is 13 m wide by 16 m high (Figure 2), with a maximum discharge capacity of 10,477 m^3/s. Along its entire length, the dam is settled in shales and sandstones, rocks that are more deformable in comparison to the concrete dam.

The lowest point of the foundation is 134.00 m above sea level, and the upper elevation is 151.75 m.a.s.l. There are seven spillways (Figure 2), each one delimited by two piers. The first and last piers have a thickness of 2.50 m, and the intermediate piers are two single of 2.5 m and four double piers of 4.0 m. On the crest, there is a vehicular concrete bridge. Also, there is a drainage and inspection gallery at an elevation of 137.00.

One year after the inauguration, inspections were carried out, and cracks were detected in different elements of the El Cuchillo Dam. In 2016, the National Water Commission (CONAGUA) started a surveying project. Topographic monuments were built for survey control data. First, a boundary monument called level bank 4 (LB-4) (Figure 1) was established and marked in a static position 3 km from the dam crest. Second, 2 level banks (LB-A and LB-B) on the concrete crest (Figure 1) are positioned 40 m away from the first and last columns. Third, 84 permanent control points (PCPs) were established in the spillways area (Annex 1). The surveying team used these marks to monitor the displacements of this dam.

Water level and environmental temperature are two factors that need to be considered for dam monitoring. Research by Dardanelli et al. indicates that displacements can be revealed in time and periodicity if it is correlated to the water level [34]. Such deformations could change during emptying and filling periods and are indicated by some authors as hysteresis loops [35]. Other researchers have found a linear relationship between water levels and dam deformations [21, 34]. The influence of seasonal concrete temperature oscillations can also impact deformations of the dam crest [36].

2.2. Monitoring of Displacements on El Cuchillo Dam with GPS Measurements. This study proposes an innovative method that can measure horizontal and vertical displacements, mapping them into optional 2D or 3D models for deformational and motion control where the required precision is millimetric [22, 27, 28]. The general workflow is displayed in Figure 3.

2.2.1. Data Acquisition, Specifications, and Preparation.
(1) Geodetic and Topographic High-Leveling Surveys. From left to right, Figure 3 explains the use of geodetic and topographic high-leveling surveys that can assess the longitudinal and transversal displacements of the crest and the correlation to the levels of the official reservoir records. For these tasks, the following devices and procedures are required. First, a Sokkia GRX2 (GPS, Glonass, Galileo, Beidou, SBAS) was used with

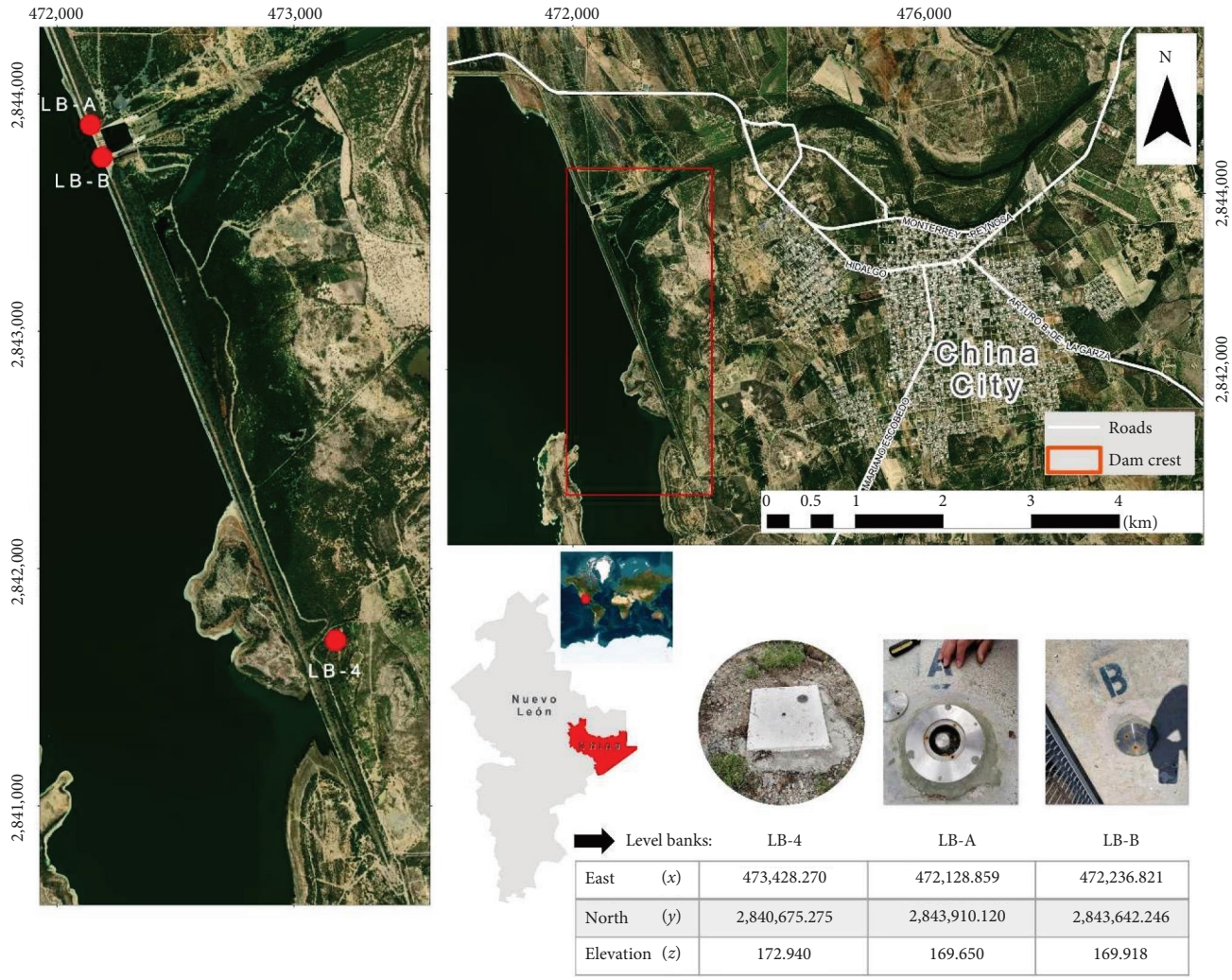

Figure 1: El Cuchillo Dam location and permanent level banks points. *Source*: World Geodetic System 1984. EPSG:32614.

Figure 2: View of the reservoir, the control structure, and the buffer tank, as well as the embedding of the lateral abutments with the dam embankment.

the following parameters: Antenna GRX1y GX2, Universal Transversal Mercator (UTM) zone 14, 102 w−96 w, static method, Ephemerid GPS, Geoid mex97c, Mask 13°, datum WGS84, and UTC-6 : 00 Guadalajara, Mexico City, Monterrey. Second, Magnet Field software is used to enter the collected positions for LB-4. The evaluation assessed the position and precision in static mode: only L1-H = 3 mm + 0.8 ppm and V = 4 mm + 1.0 ppm. Then, the superficial level banks (LB-A and LB-B) were measured with the GPS, and a double verification was conducted with a total station and a high-leveling measurement (HLM) device. The data from LB-4, LB-A, and LB-B were registered for 2 hr to obtain better data quality and precision.

The Wide Area Augmentation System (WAAS) method was used. The WAAS provides extremely accurate navigation capability by augmenting GPS, and it covers most of the United States National Airspace System (NAS) as well as parts of Canada and Mexico. This method references stations located at known points that create correction messages sent to various satellites and then broadcast to end users. Two algorithms for correction were calculated in Magnet Field: PDOP (Position 3D Dilution of Precision), this value represents the effect of the geometry of the satellites on the resulting precision, and GDOP (Geometric Dilution of Precision), which is a dimensionless number, measuring satellite geometry. Another three superficial control points were measured

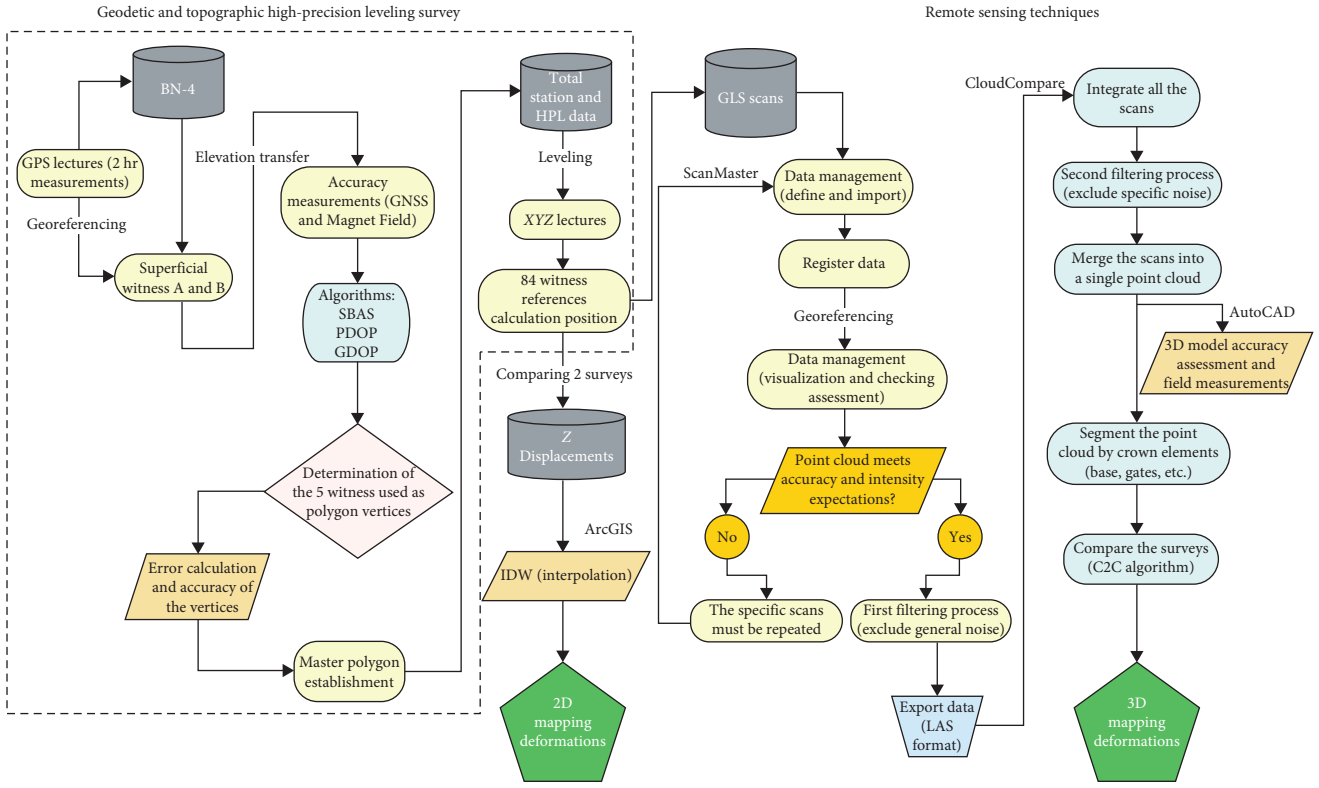

Figure 3: The workflow for the 2D and 3D mapping displacement method.

Table 1: Coordinates used to build the master polygon.

SCP	Coordinates	
Vertices (LB and PCP)	*X*	*Y*
V1 (LB-B)	472,211.948	2,843,702.639
V2 (PCP-84)	472,219.635	2,843,747.305
V3 (PCP-7)	472,176.891	2,843,853.632*
V4 (LB-A)	472,139.686	2,843,883.873
V5 (PCP-29)	472,168.162*	2,843,798.630*

Note: *These measurements presented 1 mm difference for the second survey.

using a total station Sokkia CX-101 with an accuracy of ± 1.0 mm and a mean error of ± 1.0 mm/km for the horizontal readings. Automatic Level Machine Topcon AT-B4A with 28x magnification was used to measure vertical coordinates with an accuracy of ± 2.0 mm and a mean error of ± 2.0 mm/km.

(2) Master Polygon Establishment. Using the five superficial control points (SCPs) on the dam crest, a master polygon was calculated as a reference plane. The vertices mentioned in Table 1 define the master polygon. Finally, distances among the vertices were calculated using Equation (1):

$$D = \sqrt{(x_{t-84} - x_{v-1})^2 + (y_{t-84} - y_{v-1})^2}, \quad (1)$$

which results in the following: distance from *V1* to *V2* = 45,323 m, distance from *V2* to *V3* = 114,596 m, distance from *V3* to *V4* = 47,945 m, distance from *V4* to *V5* = 89,874 m, distance from *V5* to *V1* = 105,507 m, and traverse perimeter = 403,245 m.

Error calculation of the master polygon uses the assumption that the closing error obtained in the field is the verification of the coordinates positioning the total station in two vertices. In this case, these two vertices were *V1* and LB-B Table 1). The results were as follows: in *X*-direction = 0.000 and in *Y*-direction = 0.003. With these results, the linear closing error was calculated with Equation (2):

$$el = \sqrt{eX^2 + eY^2} = \sqrt{(0.000)^2 + (0.003)^2}, \quad (2)$$

which results in a linear error: $el = 0.003$.

The final accuracy for the master polygon (Figure 4) was calculated using the maximum available precision, e.g., about 1/10,000, using Equation (3):

$$P = \frac{1}{\frac{\text{perimeter}}{el}} = \frac{1}{\frac{403.245\ \text{m}}{0.003}} = 134,415. \quad (3)$$

Therefore, 134,415 > 10,000, and thus, it meets the required precision and linear tolerance of a high-accuracy survey.

(3) 2D Mapping Displacements by an Interpolation Method. The objective of any 2D mapping is to estimate the value of the unmeasured locations based on a finite set of measurements. Inverse distance weighted (IDW) interpolation determines cell values using a linearly weighted combination of a

Figure 4: Master polygon and the control points. *Source*: World Geodetic System 1984. EPSG:32614.

set of sample points [37]. The weight is a function of the inverse distance. This method assumes that the variable being mapped decreases in influence with distance from its sampled location.

The dam displacements were mapped using ArcGIS 10.8, applying the IDW method (Equation (5)). The estimation of the z-value at location x is a weighted mean of nearby measured values:

$$z(x) = \frac{\sum_i^n W_i Z_i}{\sum_i^n W_i}, \tag{4}$$

where

$$W_i = |x - x_i|^{-\beta}, \tag{5}$$

and where $\beta \geq 0$ and $|.|$ or $|x - x_i|$ corresponds to the Euclidean distance. The inverse distance power β determines the degree to which the nearest points are preferred over more distant points.

Typically, $\beta = 1$ or $\beta = 2$ corresponds to an inverse or inverse squared relationship. The number of surrounding points n decides whether a global or local weighting is applied. Both parameters may be fine-tuned by cross-validation, a technique we discuss in the subsequent sections in more detail. If the point x coincides with a control point ($x = x_i$), then the observed value x is returned to avoid infinite weights.

(4) 3D Mapping Displacements by a Cloud-to-Cloud Comparison Method. To achieve a very high density point cloud, a detailed scanning was required to cover the entire structure using stepwise horizontal and vertical GLS. The device weight is approximately 48 kg including the GLS, batteries, tripod, and operation computer. A total of 45 scans were needed to complete the 3D model of the dam crest. This survey was repeated twice during 2021; at least 88% of the stations were located inside the master polygon. A tripod was used to position the instrument about 1.5 m above the ground. Different opening angles were used, ranging from 180 to 360° of horizontal sweep (depending on the section of the structure) and 70° of vertical sweep. The distance from the target ranged from 5 to 70 m, adjusting the resolution for all scans to 0.002 m.

Every scan was set on the highest possible angular resolution, resulting in point clouds of 70,000–170,000 points on the farthest section. The variation in point density was assumed to result from a difference in range, wind, temperature, and humidity on both the target and air [38]. The total scanned area was 1.6 ha, which resulted in a 3D point cloud with over 680 million points. Topcon ScanMaster software was used next for data processing, which involved filtering and noise removal to reduce the density and size of the data and then georeferencing [39]. The produced 3D point clouds are computationally intensive and thus challenging due to the need for computing power and memory.

2.2.2. Validation. The full 3D model was integrated to discard points that do not belong to the structure, such as noise. Validation of metric precision was realized by measuring five sections in the field using the total station and a measuring tape. Also, the digital point cloud was imported to AutoCAD 2015 and to CloudCompare V2 (CC) software to do the digital metric analysis [32].

The two surveys made in 2021 were processed using the CC software. The set of scans obtained in each surveying campaign was merged to have a complete, detailed 3D survey. After that, the CC software was also useful for splitting the complete point cloud into sections, and this is a strategy to save time and computational resources. In the second step, a filtering process was done by using the segmentation tool. Once the whole cloud was sectioned, the cloud-to-cloud (C2C) algorithm was used to compute distances between the first and second clouds using these data. The resulting 3D model generated from the first survey was considered a reference cloud, while the second (displaced cloud) was used as the comparison clouds. C2C computes the Euclidean distance using the nearest neighboring distance. It also uses a referenced cloud (the 2016 survey) and estimates the distance for each point of the subsequent compared cloud(s).

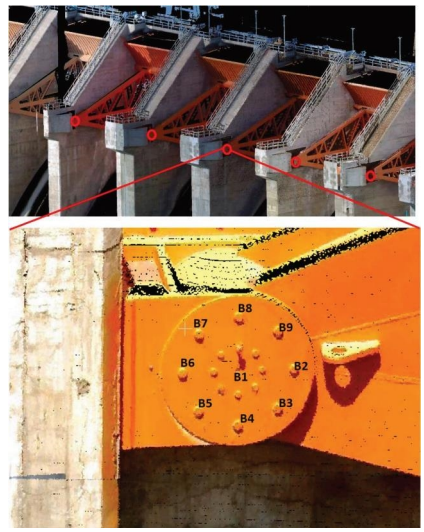

Figure 5: Zoom in of a trunnion gate and the nine measured bolts.

Each Tainter gate has two trunnions (left and right), and each one has nine marked bolts (Figure 5). A more detailed procedure was followed for the geometrical analysis of the trunnions. First, the latitude (x), longitude (y), and altitude (z) value coordinates for the 126 bolts (identified in the 14 existing trunnions) were obtained. A database was created to carefully classify the values by gate and trunnion. For each one of these, the distance among each pair of bolts was calculated.

The distance between any pair of bolts was calculated using Equation (6):

$$AB = \sqrt{(x_2 - x_1)^2 + (y_2 - y_1)^2 + (z_2 - z_1)^2}. \tag{6}$$

3. Results

3.1. Surveying. A total of four surveys were conducted during a period of 5 years using the synergy of two high-leveling and close-range remote data sensors. The water level of the reservoir in m.a.s.l. and the filling volume in mm^3 are reported in Table 2.

3.2. Validation. Specific distances of the digital 3D model obtained from the point cloud were verified in the field. These results are presented in Table 3, which allowed us to validate the model. According to the verification, the mean

Table 2: Reservoir levels and filling volume registered by CONAGUA.

	Surveying			
	First (base)*	Second	Third**	Fourth
GLS surveys	4-Sep-16	23-Jan-18	31-Jul-21	13-Sep-21
Reservoir level (m.a.s.l.)	160.92	159.67	157.72	157.56
Filling volume (mm^3)	951.15	812.42	625.71	612.72

*Referenced point cloud for the 2D model and **referenced point cloud for the 3D model.

Table 3: Differences of distances (in meters) measured between the total station and the scanner.

Measured section	Total station	3D digital model	Absolute differences
Pier 10–11	2.945	2.9466	0.00160
Pier 9	1.424	1.4247	0.00070
Pier 2–3	2.958	2.9596	0.00160
Pier 7–8	2.896	2.8944	0.00160
WT 64–71	1.4978	1.4956	0.00220
Mean	—	—	0.00154
Standard deviation	—	—	0.00054

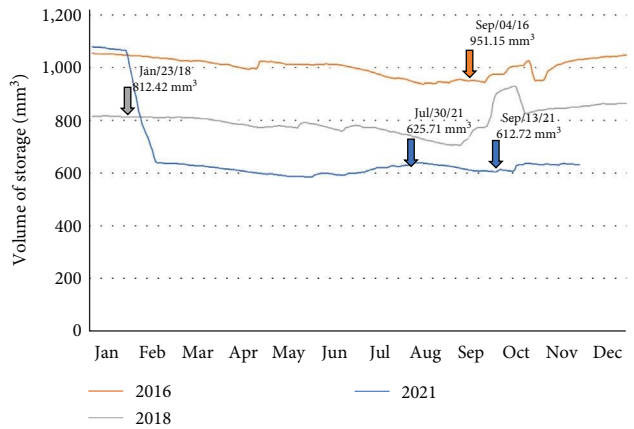

Figure 6: Storage volume of the Cuchillo Dam during the three evaluated surveys (5-year monitoring period).

value of the error is 0.00154 m and a standard deviation of 0.0005 m, similar to that reported by [40].

3.3. Fill Level and Deformation of El Cuchillo Dam. The values of the storage volume during the 5 years of the study (Figure 6) and the hydrostatic pressure over the dam could be correlated with the measured dam kinematics.

3.3.1. 2D Mapping Displacements. The altimetry differences in the structure revealed a deformation pattern over the crown of the dam, consisting of both uplift and subsidence areas. The total measured differences in the field go up to 11 mm (uplift) at the left riverbank to −5 mm (subsidence) from the middle part to the right riverbank, specifically in longitudinal section 7, where the trunnions are located. Piers 5–9 present the most consistent subsidence in the order of −7.3 mm in piers 5 and 6. Conversely, in both LB-A and above gate 3, there are uplifts up to 12 mm (Figure 7).

3.3.2. 3D Mapping Displacements. The digital 3D model, aligned and validated, allows an understanding of the kinematic behavior of the central axis of the trunnion gates. The change of position was used to monitor the longitudinal and transversal displacements. The results indicate that the displacements can rise to 6.272 cm among the trunnion central bolts of gate 1 and gate 4 (156.72 m–156.78 m) (Figure 8) along the monitored period.

In Figure 9, the 3D displacements over the dam crest can be observed in a colored code (blue to red). Using CloudCompare software to visualize these results, the whole range of possibilities that this provides can be more appreciated. With the comparison of the 2021 3D datasets, the horizontal displacements are observed not only in the aerial view but also in a perpendicular view. In Figure 9, displacements up to 4 mm can be observed all over the left face of pier 6.

4. Discussion

This type of study, which employs high-precision leveling techniques and short-range laser remote sensors to assess displacements in structures such as dams, provides several significant contributions, such as monitoring of critical structures such as dams, identification of *xyz* displacements, temporal analysis, model validation, relationship with filling fast conditions, and early warning.

This research evaluated four datasets obtained using high-precision leveling and laser close-range remote data sensing, and two assessments were done. The first assessment was done using 84 control points during a 5-year period of study producing 2D displacement maps. Due to the relatively long period of measurements, the observed displacements were larger than the normal errors.

On the other hand, the second assessment was done in a period of 2 months (Table 2), with the digital 3D point cloud producing a very high-resolution cloud. However, the results

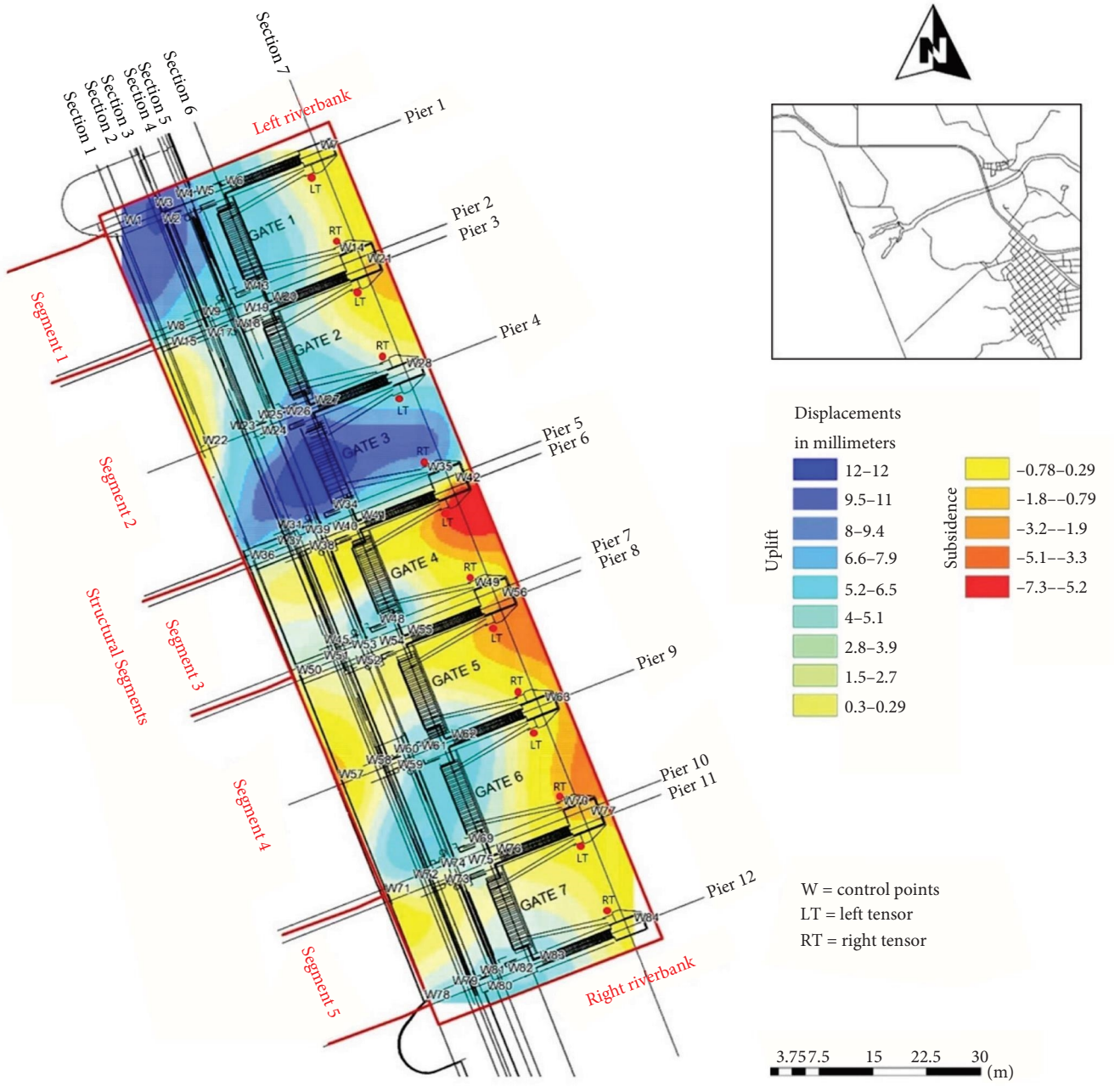

Figure 7: Displacement in Z-direction of the crown, based on the IDW method between 2016 and 2021.

indicate that the differences did not exceed 3 mm, which means that the results are not significant, considering that the error range of the measuring instruments has a normal error of ± 3 mm.

According to the geometric evidence of the "El Cuchillo-Solidaridad" Dam, the structure has allegedly shown continuous displacements since its first years after its construction in 1994. Until 2021, displacements up to 6.27 cm have been measured. The vertical displacements are represented by uplifts on the left dam stirrup and subsidence along cross-section 7. The average annual displacement is 1.16 mm, and two specific points from piers 5 and 10 had cracks up to 2.34 cm. These displacements can have implications for the safety and integrity of the dam, and knowledge of these movements is essential for informed decisions regarding maintenance and repairs. Comparing the differences in elevations of the 84 control points over a 5-year period (2016 vs. 2021), the temporal analysis reveals shifts of up to 11 mm. These displacements mark a trend of 11 mm uplifts on the left riverbank, mainly from pier 1 to pier 5, and subsidences of up to −5 mm from piers 6–11, especially in section 7.

The dam filling conditions during the 5-year monitoring period decreased from 951.15 mm^3 in September 2016 to 612.72 mm^3 in September 2021. According to the measured

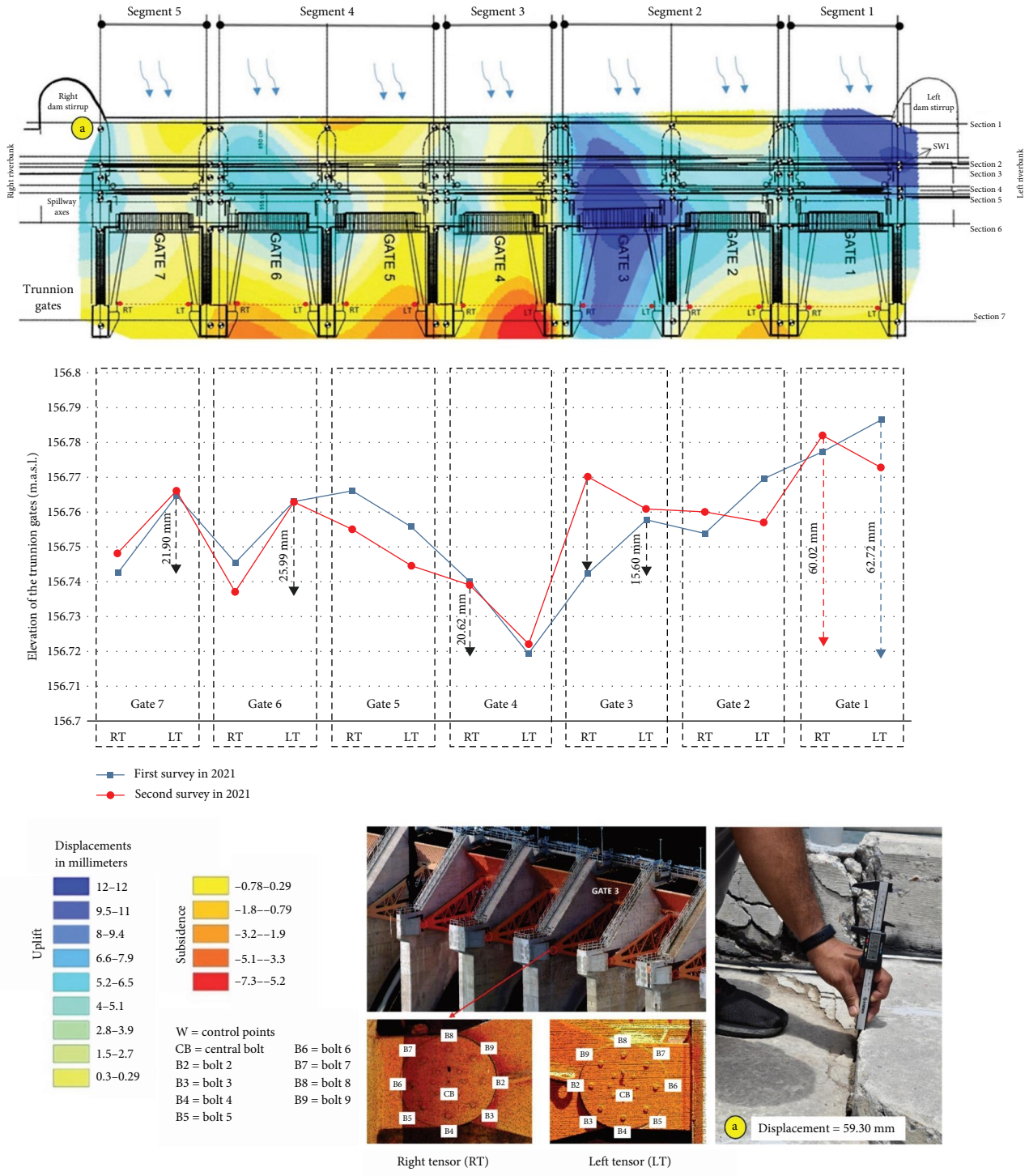

FIGURE 8: Mapping the displacements in the *Z*-direction of the crest dam, taking into consideration the differences among the control points between the 2016 base survey and the 2021 final survey.

displacements, there could be a relationship between the fill level conditions and the longitudinal and vertical displacements. However, the methodology of high-precision remote sensing was the same.

By linking displacements with dam filling conditions, these studies can contribute to understanding the influence of water level on structural movements, which is highly relevant for dam design and management. However, detailed and continuous monitoring of this dam is crucial to ensure safety and stability over time. On the other hand, the data collected to date can be used to validate theoretical and numerical models of structural behavior, improving understanding of the actual conditions of the dam and the accuracy of predictions. Moreover, early warning is a very important contribution of this

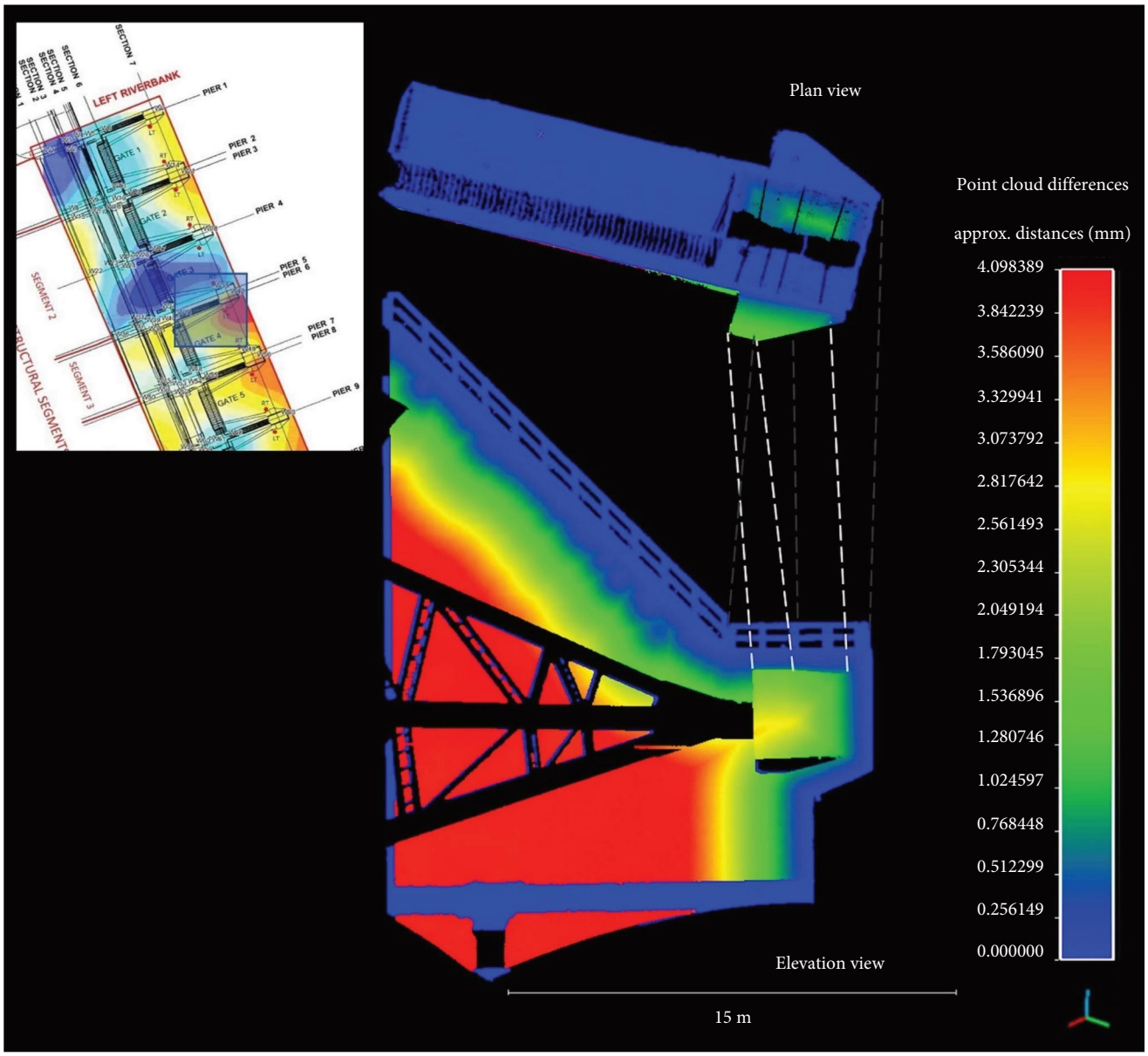

Figure 9: Mapping 3D displacements using absolute distances between the two 2021 surveys.

work; these studies serve as a valuable tool for early detection of potential structural issues. The ability to identify displacements even before they reach critical levels can be crucial for making preventive decisions. In summary, studies employing these techniques offer essential information for the management, maintenance, and security of critical infrastructures such as dams, contributing to informed decision-making and the prevention of potential risks.

5. Conclusions

Reservoirs as the "El Cuchillo" Dam are essential infrastructure assets, and they require both a more decisive and stricter displacement monitoring program. The use of remote sensing technologies as high-precision leveling and laser scanning, together with more traditional sensing technologies, can provide much more reliable information about dam kinematics; This type of study, however, could have some limitations in a field, such as the time-consuming, heavy equipment or computational challenges. This way, the decision-makers can make better judgements. Three conclusions emerge from this study:

(i) First, "El Cuchillo" Dam displaced 1.16 mm annually since 1994. 2D and 3D maps identify and locate displacements of 11 mm uplifts on the left riverbank, mainly from pier 1 to pier 5, and subsidences of up to −5 mm from piers 6 to 11, especially in section 7.

(ii) Both the 2D and 3D models revealed similar altitudinal displacements in the upper part, as in the case of piers 5–9, present the most consistent subsidence in the order of −7.3 mm piers 5 and 6; however, the

dam curtain is moving in the three axes. Longitudinal and transverse displacements are visible in (a) the opening of the joints between the head and the slab sections of the vehicular bridge and (b) the garnish and railing of the upstream end of the bridge vehicular bridge and opening of the joints and displacement of the gasket of the lower rest of ramp of stairs in double stacks, and in two specific points of piers 5 and 10 where cracks are up to 2.34 cm.

(iii) Finally, in further research of "El Cuchillo" Dam, it is important to consider (1) a stricter experiment design, mainly under different filling dam scenarios and thermal fluctuations due to seasonal differences; (2) explore remote sensing InSAR analysis, which is a cost-effective method for displacement measurement at dams and reservoir banks [41], and since this dam was built in 1994, it must be possible to find historical images [42]; and (3) integrate geological and geotechnical information under the dam structure to know the type of rock formation, along with its physical and mechanical properties. In this study, this information was not available. Thus, it will be necessary to carry out a geological exploration campaign.

Data Availability

The point cloud data used to support the findings of this study were supplied by under license. Requests for access to these data should be made to Jaime Gudiño, jaime.gudino@conagua.gob.mx.

Conflicts of Interest

The authors declare no conflicts of interest.

Authors' Contributions

Fabiola D. Yépez-Rincón was responsible for conceptualization. Fabiola D. Yépez-Rincón and Andrea N. Escobedo Tamez were responsible for data curation. Fabiola D. Yépez-Rincón was responsible for formal analysis and technoproject. Adrián L. Ferriño Fierro and Luis C. Alatorre Cejudo were responsible for funding acquisition. Fabiola D. Yépez-Rincón was responsible for investigation. Fabiola D. Yépez-Rincón, Andrea N. Escobedo Tamez, and Olmo Pinedo Sandoval were responsible for methodology. Víctor H. Guerra Cobián was responsible for project administration. Fabiola D. Yépez-Rincón and Olmo Pinedo Sandoval were responsible for software. Fabiola D. Yépez-Rincón was responsible for validation, visualization, and writing of the original draft. Jorge H. Chávez Gómez and Saied Pirasteh were responsible for writing and reviewing and editing. All authors have read and agreed to the published version of the manuscript.

Acknowledgments

The authors sincerely thank the CONAGUA, Civil Engineer Institute of the UANL and Technoproject SA de CV. This research was funded by the National Water Commission, grant number 2021-B05-B32-CA-19-RF-I3-A-OR-0020.

References

[1] F. I. Arreguín-Cortés, R. Murillo-Fernández, and H. Marengo-Mogollón, "Inventario nacional de presas," *Tecnología y Ciencias del Agua*, vol. 4, no. 4, pp. 179–185, 2013.

[2] L. Yang, M. Liu, J. A. Smith, and F. Tian, "Typhoon Nina and the August 1975 flood over central China," *Journal of Hydrometeorology*, vol. 18, no. 2, pp. 451–472, 2017.

[3] L. Yang, L. Wang, P. Lu, X. Li, and J. Gao, "Extreme rainfall and inland flooding associated with landfalling tropical cyclones over China," in *AGU Fall Meeting Abstracts*, pp. H33K–2093, American Geophysical Union, 2019, Dec.

[4] M. Scaioni, M. Marsella, M. Crosetto, V. Tornatore, and J. Wang, "Geodetic and remote-sensing sensors for dam deformation monitoring," *Sensors*, vol. 18, no. 11, Article ID 3682, 2018.

[5] D. A. Zaldivar-Salinas, "Análisis de esfuerzos, deformaciones y desplazamientos en presas de enrocamiento con cara de concreto por medio del método del elemento finito," Tesis de Maestría en Ingeniería Civil y Geotecnia. Universidad Nacioanl Autónoma de México. 130, 2008.

[6] A. Sivasuriyan, D. S. Vijayan, R. Munusami, and P. Devarajan, "Health assessment of dams under various environmental conditions using structural health monitoring techniques: a state-of-art review," *Environmental Science and Pollution Research*, vol. 29, no. 57, Article ID 86180, 2022.

[7] F. D. Yépez-Rincón, J. H. Chávez-Gómez, A. L. Ferriño-Fierro, J. J. Aguilar-Durán, and H. J. Sánchez-Gaytán, "Análisis espectral de materiales y geometría de muros existentes previo a la aplicación de cargas," 2020.

[8] W. Wiedemann and C. Holst, "Identifying individual rocks within laser scans for a rigorous deformation analysis of water dams," in *5th Joint International Symposium on Deformation Monitoring (JISDM)*, pp. 327–334, Editorial Universitat Politècnica de València, Valencia, Spain, 2022, June.

[9] C. Lin, T. Li, S. Chen, X. Liu, C. Lin, and S. Liang, "Gaussian process regression-based forecasting model of dam deformation," *Neural Computing and Applications*, vol. 31, no. 12, pp. 8503–8518, 2019.

[10] D. Proske, "Comparison of dam failure frequencies and failure probabilities," *Beton- und Stahlbetonbau*, vol. 113, no. S2, pp. 2–6, 2018.

[11] T. Collins, *Ageing Dams Pose Growing Threat*, United Nations University, 2023.

[12] Z. Zhongming, L. Linong, Y. Xiaona, Z. Wangqiang, and L. Wei, "Retiring ageing hydropower dams could protect people and budgets," But aren't they needed in the energy transition? FEMA. 2015, 2021.

[13] Federal Emergency Management Agency, "Federal guidelines for dam safety risk management. FEMA P-1025," US Department of Homeland Security, Washington (DC), 2015.

[14] H. Chen, "Seismic safety of high concrete dams," *Earthquake Engineering and Engineering Vibration*, vol. 13, no. S1, pp. 1–16, 2014.

[15] P. Bukenya, P. Moyo, H. Beushausen, and C. Oosthuizen, "Health monitoring of concrete dams: a literature review," *Journal of Civil Structural Health Monitoring*, vol. 4, no. 4, pp. 235–244, 2014.

[16] S. Kibret, M. McCartney, J. Lautze, L. Nhamo, and G. Yan, "The impact of large and small dams on malaria transmission in four basins in Africa," *Scientific Reports*, vol. 11, no. 1, pp. 1–12, 2021.

[17] Conagua, "Water statistics, 2011 (in Spanish)," Comisión Nacional del Agua, México, DF, 2011.
[18] Y. Kalkan, "Geodetic deformation monitoring of Ataturk Dam in Turkey," *Arabian Journal of Geosciences*, vol. 7, no. 1, pp. 397–405, 2014.
[19] P. Michalis, S. I. Pytharouli, and S. Raftopoulos, "Long-term deformation patterns of earth-fill dams based on geodetic monitoring data: the Pournari I Dam case study," in *Proceedings of the 3rd Joint International Symposium on Deformation Monitoring (JISDM)*, vol. 30, pp. 1–5, JISDM, Vienna, Austria, 2016, March.
[20] S. Grosel, "Numerical analysis of tailing dam with calibration based on genetic algorithm and geotechnical monitoring data," *Studia Geotechnica et Mechanica*, vol. 43, no. 1, pp. 34–47, 2020.
[21] C. O. Yigit, S. Alcay, and A. Ceylan, "Displacement response of a concrete arch dam to seasonal temperature fluctuations and reservoir level rise during the first filling period: evidence from geodetic data," *Geomatics, Natural Hazards and Risk*, vol. 7, no. 4, pp. 1489–1505, 2016.
[22] D. Galán-Martín, R. Martínez-Marín, M. Marchamalo-Sacristán, and J. A. Sánchez-Sobrino, "Control de movimientos en presas mediante DGPS: aplicación a la presa de La Aceña, España," *Tecnología y Ciencias del Agua*, vol. 2, no. 3, pp. 159–176, 2011.
[23] J. R. Vazquez-Ontiveros, C. A. Martinez-Felix, G. E. Vazquez-Becerra, J. R. Gaxiola-Camacho, A. Melgarejo-Morales, and J. Padilla-Velazco, "Monitoring of local deformations and reservoir water level for a gravity type dam based on GPS observations," *Advances in Space Research*, vol. 69, no. 1, pp. 319–330, 2022.
[24] Q. Wang, W. Shi, and P. M. Atkinson, "Sub-pixel mapping of remote sensing images based on radial basis function interpolation," *ISPRS Journal of Photogrammetry and Remote Sensing*, vol. 92, pp. 1–15, 2014.
[25] I. Ashraf, S. Hur, and Y. Park, "An investigation of interpolation techniques to generate 2D intensity image from LIDAR data," *IEEE Access*, vol. 5, pp. 8250–8260, 2017.
[26] X.-Y. Yin, O. Mercier, B. Yadav, K. Schneider, and J.-C. Nave, "A characteristic mapping method for the two-dimensional incompressible Euler equations," *Journal of Computational Physics*, vol. 424, Article ID 109781, 2021.
[27] D. Poreh and S. Pirasteh, "InSAR observations and analysis of the medicina geodetic observatory and CosmoSkyMed images," *Natural Hazards*, vol. 103, no. 3, pp. 3145–3161, 2020.
[28] D. Poreh, S. Pirasteh, and E. Cabral-Cano, "Assessing subsidence of Mexico city from InSAR and LandSat ETM+ with CGPS and SVM," *Geoenvironmental Disasters*, vol. 8, Article ID 7, 2021.
[29] K. Chen, G. Liu, W. Xiang et al., "Assimilation of SBAS-InSAR based vertical deformation into land surface model to improve the estimation of terrestrial water storage," *IEEE Journal of Selected Topics in Applied Earth Observations and Remote Sensing*, vol. 15, pp. 2826–2835, 2022.
[30] D. González-Aguilera, J. Gómez-Lahoz, and J. Sánchez, "A new approach for structural monitoring of large dams with a three-dimensional laser scanner," *Sensors*, vol. 8, no. 9, pp. 5866–5883, 2008.
[31] H. Xu, H. Li, X. Yang, S. Qi, and J. Zhou, "Integration of terrestrial laser scanning and NURBS modeling for the deformation monitoring of an earth-rock dam," *Sensors*, vol. 19, no. 1, Article ID 22, 2019.
[32] Y. Li, P. Liu, H. Li, and F. Huang, "A comparison method for 3D laser point clouds in displacement change detection for arch dams," *ISPRS International Journal of Geo-Information*, vol. 10, no. 3, Article ID 184, 2021.
[33] V. H. Guerra-Cobián, A. L. Ferriño-Fierro, F. D. Yépez-Rincón, R. A. Cavazos-González, and J. D. D. Rodríguez-Rodríguez, "Status of regional drinking water services in Nuevo Leon, Mexico," in *Water Availability and Management in Mexico*, vol. 88 of *Water Science and Technology Library*, pp. 323–349, Springer, Cham, 2020.
[34] G. Dardanelli, G. La Loggia, N. Perfetti, F. Capodici, L. Puccio, and A. Maltese, "Monitoring displacements of an earthen dam using GNSS and remote sensing," in *Remote Sensing for Agriculture, Ecosystems, and Hydrology*, vol. 9239, pp. 574–589, SPIE, Amsterdam, Netherlands, 2014, October.
[35] C. Pipitone, A. Maltese, G. Dardanelli, M. Lo Brutto, and G. La Loggia, "Monitoring water surface and level of a reservoir using different remote sensing approaches and comparison with dam displacements evaluated via GNSS," *Remote Sensing*, vol. 10, no. 1, Article ID 71, 2018.
[36] S. Alcay, C. O. Yigit, C. Inal, and A. Ceylan, "Analysis of displacement response of the Ermenek dam monitored by an integrated geodetic and pendulum system," *International Journal of Civil Engineering*, vol. 16, no. 10, pp. 1279–1291, 2018.
[37] C. Childs, "Interpolating surfaces in ArcGIS spatial analyst," *ArcUser*, vol. 3235, no. 569, pp. 32–35, 2004.
[38] F. D. Yépez-Rincón, L. Luna-Mendoza, N. L. Ramírez-Serrato, A. Hinojosa-Corona, and A. L. Ferriño-Fierro, "Assessing vertical structure of an endemic forest in succession using terrestrial laser scanning (TLS). Case study: Guadalupe Island," *Remote Sensing of Environment*, vol. 263, Article ID 112563, 2021.
[39] A. F. Razali, M. F. M. Ariff, and Z. Majid, "A hybrid point cloud reality capture from terrestrial laser scanning and UAV-photogrammetry," *The International Archives of the Photogrammetry, Remote Sensing and Spatial Information Sciences*, vol. XLVI-2/W1-2022, pp. 459–463, 2022.
[40] K. P. Dampegama, J. M. I. Karalliyadda, and K. P. Manuranga, "Assessing the accuracy of terrestrial laser scanner against the total station for surveying applications in Sri Lanka," 2020.
[41] D. Roque, J. N. Lima, D. Perissin, A. P. Falcão, J. V. Lemos, and A. M. Fonseca, "Integrated InSAR and GNSS monitoring subsystem for an arch dam and reservoir banks," *Journal of Surveying Engineering*, vol. 147, no. 3, Article ID 05021003, 2021.
[42] H. Duan, Y. Li, H. Jiang et al., "Retrospective monitoring of slope failure event of tailings dam using InSAR time-series observations," *Natural Hazards*, vol. 117, no. 3, pp. 2375–2391, 2023.